

Offset Sampling Improves Deep Learning based Accelerated MRI Reconstructions by Exploiting Symmetry

Aaron Defazio
Facebook AI Research NY, fastMRI team

Abstract

Deep learning approaches to accelerated MRI take a matrix of sampled Fourier-space lines as input and produce a spatial image as output. In this work we show that by careful choice of the offset used in the sampling procedure, the symmetries in k-space can be better exploited, producing higher quality reconstructions than given by standard equally-spaced samples or randomized samples motivated by compressed sensing.

1 Problem setup

Deep learning based accelerated MRI reconstruction methods are typically trained using supervised machine learning. Our work uses the recently released fastMRI multi-coil dataset [Zbontar et al., 2018], which consists of a set of raw k -space data $x^{(j)}$ in multi-dimensional arrays : $n_c \times h \times w$. From this data a ground-truth image $m^{(j)}$ is produced, using a direct IFFT followed by a standard sum-of-squares approach to combing coil images.

These training pairs are then used to train a black box model B (typically a neural network), which maps from raw subsampled k-space tensors to $h \times w$ spatial images. For instance, the training loss for data-point j is given by:

$$L^{(j)}(\phi) = SSIM \left(B_{\phi} \left(M \left(x^{(j)} \right) \right), m^{(j)} \right),$$

where M is a masking function that zeros out a fraction of the k -space lines, simulating a subsampling process. This work is primarily concerned with the choice of masking function M . Due to the physics of the MRI acquisition process, the mask is the same for each coil, and it is most efficient to capture full rows or columns at a time. For the purposes of discussion we will consider the simplified case of a 1D FFT, with a single channel, as this captures the important aspects of the sampling processes. The same sampling mask may be extended to 2D images and multiple coil channels by duplicating the mask for each coil, and extending the mask along the additional spatial dimension to capture full lines of k-space.

2 1D FFT Notation

We call the *image-space* image the magnetization image $x(n)$, of width N , and it's Fourier transform the *k-space* image $X(k)$, also of width N . The (1D) DFT is defined as:

$$X(k) = \sum_{n=0}^{N-1} x(n) \exp(-2\pi i k n / N)$$

and the IFT is:

$$x(n) = \sum_{k=0}^{N-1} X(k) \exp(2\pi i k n / N).$$

3 Equispaced Sampling

A naive application of equispaced sampling is to form the masked k-space Y from the unmasked space X via:

$$Y(k) = \begin{cases} X(k) & k \bmod R = 0 \\ 0 & \text{otherwise} \end{cases}$$

Where R is the subsampling factor, or acceleration factor.

The behavior of the masking operation is interesting. It results in the IFFT $y(m) = IFFT(Y(k))$ containing R copies of $x(m)$, the true magnetization image, each offset by N/R from the last, for width N .

$$y(m) = \frac{1}{R} \sum_{r=0}^{R-1} x(m + rN/R)$$

by convention indexing of images is modulo the image size, so these duplicates wrap at the image boundaries (Figure 1b). We focus on the case where the k-space width is a multiple of R , as otherwise the offsets rN/R do not align with pixel boundaries. This is known as aliasing in the Fourier literature, and in particular this masking operation can be considered the composition of a DOWNSAMPLE operation followed by a STRETCH operation. A model must thus “decode” this image by disentangling the R pixels that sum at each location.

We can provide a potentially more useful image to the model by considering instead a sampling mask shifted by a single pixel:

$$Y(k) = \begin{cases} X(k) & k \bmod R = 1 \\ 0 & \text{otherwise} \end{cases}.$$

A remarkable property of this mask is that the shifted copies of the image are now no longer in-phase but rather each differs by a phase of $2\pi/R$ radians:

$$y(m) = \frac{1}{R} \sum_{r=0}^{R-1} x(m + rN/R) \exp(2\pi r/R)$$

This offset-1 sampling mask has a number of advantages, particularly for the $R = 4$ case which is of particular practical interest as it provides a good balance of acceleration and reconstruction quality. The 4 phases are real-positive, imaginary-positive, real-negative and imaginary-negative.

If the magnetization image is also real-valued, then the real channel of the IFFT will contain only 2 aliased images, separated by half the image width, one positive and one equal but negated. This is effectively half the overlap from what occurs in the offset-0 case. In the case where the anatomy only takes up half the width, the two will be completely separated, resulting in a perfect reconstruction modulo noise just by clamping negative values to 0. The anatomy taking up half the width or less is not uncommon as many coils are sensitive to signals in only a portion of the field of view in common coil designs.

This shifted equispaced pattern is particularly advantageous if the signal is real-valued, since there will be less overlap in the aliased copies, as shown in Figure 1. Acceleration from exploiting the real-valued nature of a signal is known as partial Fourier [Feinberg et al., 1986, Haacke et al., 1991, McGibney et al., 1993] in the MRI literature. The offset-1 sampling scheme is able to automatically make use of conjugate symmetry when possible.

4 Phase shift derivation

The above result is easiest to show by working backwards. We start with image space:

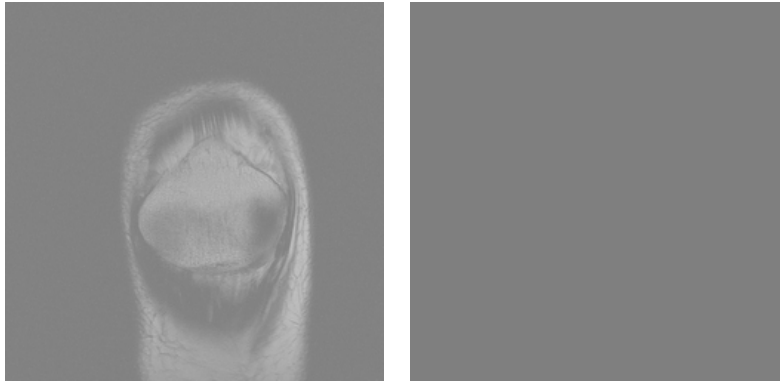
$$y(m) = \frac{1}{R} \sum_{r=0}^{R-1} x(m + rN/R) \exp(-2\pi ir/R),$$

then we take the FFT:

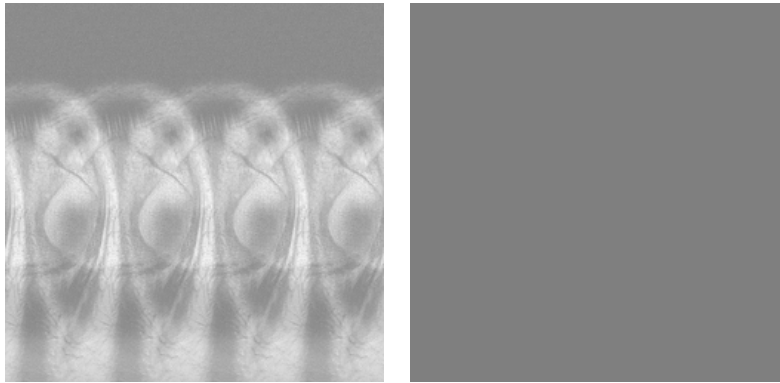
$$Y(k) = \frac{1}{R} \sum_{r=0}^{R-1} \exp(-2\pi ir/R) \sum_{n=0}^{N-1} x(n + rN/R) \exp(-2\pi ikn/N).$$

The FFT of a shifted image is equal to multiplication by a linear-phase term:

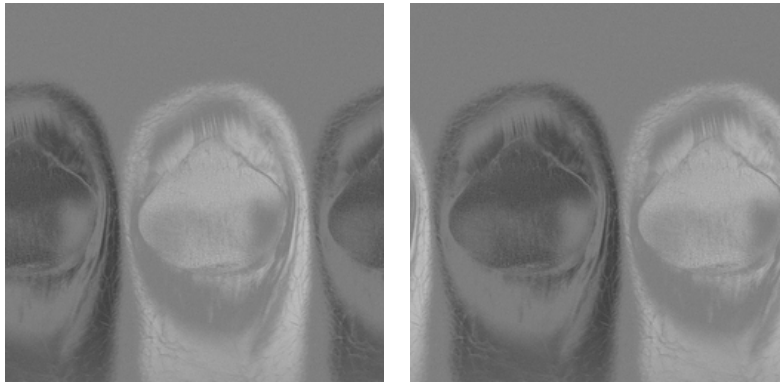
$$\mathcal{F}(x(n + a))(k) = \exp(2\pi iak/N)X(k),$$



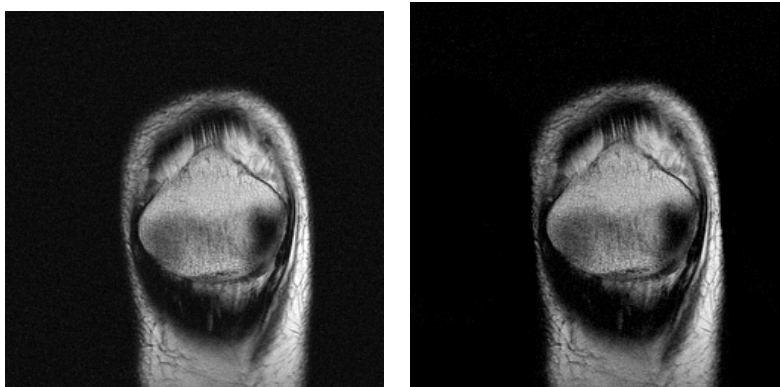
(a) Image space, with grey as 0, real & imaginary components shown



(b) Shift-0 IFFT real & imaginary components



(c) Shift-1 IFFT real & imaginary components



(d) Original (left) versus a shift-1 reconstruction (right) from clamping negative values

Figure 1: IFFTs in an idealized case, where the input is real valued and takes up less than half of the horizontal field-of-view.

so

$$\begin{aligned}
 Y(k) &= \frac{1}{R} \sum_{r=0}^{R-1} \exp(-2\pi ir/R) \exp(2\pi i (rN/R) k/N) \left[\sum_{n=0}^{N-1} x(n) \exp(-2\pi i kn/N) \right] \\
 &= \frac{1}{R} \sum_{r=0}^{R-1} \exp(-2\pi ir/R) \exp(2\pi i (rN/R) k/N) X(k) \\
 &= X(k) \cdot \left[\frac{1}{R} \sum_{r=0}^{R-1} \exp(-2\pi ir/R + 2\pi i (r/R) k) \right] \\
 &= X(k) \cdot \left[\frac{1}{R} \sum_{r=0}^{R-1} \exp(2\pi i (r/R) (k-1)) \right].
 \end{aligned}$$

The sum can be computed using sum-of-a-geometric-series machinery. Let $\omega = \exp(2\pi i/R)$ be the first root of unity. Then using the formula:

$$\sum_{r=0}^{R-1} \omega^{r(k-1)} = \frac{\omega^{R(k-1)} - 1}{\omega^{k-1} - 1} = \frac{1 - 1}{\omega^{k-1} - 1}.$$

So as long as the denominator is not zero, the sum is zero. The denominator is zero when $k-1 \pmod R = 0$ as the powers of unity wrap around at R , and in that case we have

$$\sum_{r=0}^{R-1} \omega^{r(k-1) \pmod R} = \sum_{r=0}^{R-1} \omega^0 = R.$$

The result is:

$$Y(k) = \frac{1}{R} X(k) \cdot \begin{cases} R & (k-1) \pmod R = 0 \\ 0 & \text{otherwise} \end{cases}.$$

An alternative view: exploiting conjugate symmetry

The above mathematical treatment does not shed much light on *why* using an alternative offset results in more information being retained. In this section we give a more direct argument. Consider the DFT as stored in memory. We consider a simple 1D case of width 12. The Nyquist frequency is $f = 1/6$. The standard frequency layout in memory is the following:

$$[0f \quad 1f \quad 2f \quad 3f \quad 4f \quad 5f \quad -6f \quad -5f \quad -4f \quad -3f \quad -2f \quad -f].$$

When using the regular equispaced sampling, we keep the following frequencies:

$$[0f \quad 0 \quad 0 \quad 0 \quad 4f \quad 0 \quad 0 \quad 0 \quad -4f \quad 0 \quad 0 \quad 0],$$

Now recall that for real images, the k-space component for a frequency is equal to that of the conjugate of its negative frequency. This is known as the conjugate symmetry property of the real-value FFT. So using an offset-0 sampling pattern actually keeps 2 copies of the same frequency, giving us redundant information.

In contrast, the offset-1 pattern gives:

$$[0 \quad 1f \quad 0 \quad 0 \quad 0 \quad 5f \quad 0 \quad 0 \quad 0 \quad -3f \quad 0 \quad 0]$$

So offset-1 sampling retains more frequencies, once conjugate symmetry is taken into account.

FFT shift

It is common to store and manipulate FFT data in shifted configuration, as given by the “fftshift” operation in Matlab or NumPy. This shift operation moves the low frequencies to the center of k-space, which is desirable for visualization purposes. The sampling procedure described above must be performed on unshifted data as the sampling mask will otherwise have an incorrect offset pattern. To avoid unnecessary shifting of the full data matrix, the mask can be computed assuming unshifted data, then the mask itself can be shifted to match the data’s layout.

Algorithm 1 Python code that correctly produces an offset-1 sampling mask for irregularly sized inputs

```
offset_pos = 1
offset_neg = 2
poslen = (n+1)//2
neglen = n - poslen
mask_positive = np.zeros(poslen, dtype=np.float32)
mask_negative = np.zeros(neglen, dtype=np.float32)

mask_positive[offset_pos::acceleration] = 1
mask_negative[offset_neg::acceleration] = 1
mask_negative = np.flip(mask_negative)

mask = np.concatenate((mask_positive, mask_negative))
```

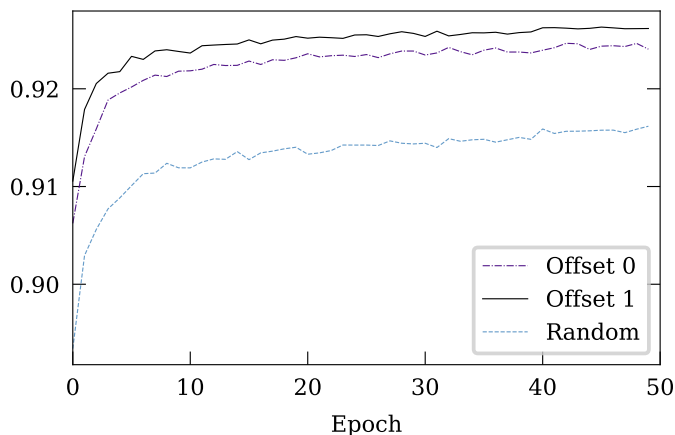


Figure 2: Comparison of offset sampling for 4x accelerated knee MRI reconstruction, showing an improvement in SSIM from 0.924 to 0.926.

Handling irregularly sized inputs.

The above theory relies on the k-space image being an exact multiple of the acceleration factor. When using non-multiples of the acceleration factor the shifted copies occur at fractional pixel locations which results in blurring. Although we strongly recommend performing scans with the width in the phase-encoding direction a multiple of the acceleration factor, it is not always practical.

To get the correct pattern for image widths that are not a multiple of the acceleration factor, the positive and negative parts of the mask should be calculated separately. In the case of acceleration factor 4, the offset for the negative part should be 2, counting backward from the end (i.e. frequencies $-3f$, $-7f$, ...). Numpy code that produces correct masks is given in Algorithm 1.

Handling phase shifts

Most practical MRI acquisitions exhibit a non-uniform and non-zero phase, so the idealized case of all real-valued images is far from the norm. Nevertheless, the described sampling mask still yields additional information when the magnetization image is close to uniform in phase. Since the masked data is input to a learned black-box model, this information can potentially be used by the model to provide improved reconstructions, without requiring any explicit partial Fourier techniques.

5 Experiments

We compared the sampling approaches by training a deep-learning-based system that takes a set of masked k-space channel images as input and produces a spatial image as output. The training procedure followed the setup and

multi-coil dataset from Zbontar et al. [2018]. We used a cascade of four U-Nets [Ronneberger et al., 2015] following Schlemper et al. [2018], although we found our results were robust to the particular reconstruction model used. The output of each U-Net is projected onto the known k-space values (via a FFT-set-IFFT operation) before the application of the next U-net. We used 4x subsampling for each mask, with the 16 lowest-frequency lines also added to each mask via an OR operation.

Training consisted of 50 epochs of ADAM method with learning rate 0.0003, $\beta_1 = 0.9$, $\beta_2 = 0.999$, batch-size 8, and no weight decay, data augmentation or other regularization. The use of offset 1 sampling significantly improves the validation SSIM, as shown in Figure 2, and is superior to both random sampling and offset 0 sampling. A set of example reconstructions from the validation set is given in the Appendix, Figures 3 to 6. Both the standard offset 0 and the proposed offset 1 methods produce good results. However, the offset 1 approach produces sharper reconstructions, with more accurate low-level details. We have highlighted regions where the differences are most prominent, but smaller differences are visible through-out. The differences are stronger when the signal-to-noise ratio is low.

6 Discussion

The use of randomized sampling for accelerated MRI has been a focus of significant research [Lustig et al., 2007] as an application of the theory of compressed sensing. It may be surprising then that our empirical results show a significant advantage to equispaced sampling. We attribute this to a violation of the assumptions of compressed sensing when applied to MRI images. For compressed sensing theory to apply, there must exist some basis in which the image is near-sparse. For the proton density scans with and without fat-suppression used in the fastMRI dataset, there is significant textural detail which are not sparse in image space or common wavelet bases. Random sampling is much better suited to other MRI scan types such as vascular MRI [Yamamoto et al., 2018], where the images are naturally sparse.

When equispaced sampling is used, the reconstruction problem becomes a problem of disentangling multiple overlapping copies of the anatomy when considered in image-space. This is a task that convolutional neural networks are well-suited for, as the information about each pixel location in the final image is localized to the neighborhood of R (for acceleration factor R) spots in the IFFT image. The cascaded U-Net architecture uses an alternating sequence of local operations (U-Nets) combined with non-local operations (projection onto known k-spaces lines) to reconstruct the image.

In contrast, when a random sampling pattern has been used the information needed to recover each location is spread throughout the image. Convolutional neural networks use small kernels that are not well-suited to aggregating information that is so spread out.

The use of offset sampling may not result in improved reconstruction quality when classical accelerated imaging [Deshmane et al., 2012] approaches such as SENSE [Pruessmann et al., 1999] or GRAPPA [Griswold et al., 2002] are used, since they do not take advantage of the conjugate symmetry present.

Conclusion

The offset-1 approach shows a clear empirical advantage over other fixed sampling approaches and is well supported by theory. The interpretation of the approach as capturing non-redundant lines in k-space between the positive and negative halves relates it to past work that exploits conjugate symmetry such as partial Fourier approaches [Feinberg et al., 1986]. While partial Fourier approaches typically fully capture the positive half and partially capture the negative half, in the accelerated setting it's possible to capture a subset of lines from both halves, as long as the frequencies differ. The offset-1 sampling mask can be seen as an extension of this idea to accelerated deep-learning-based reconstructions.

Our results suggest an interesting avenue for research: if the coil design is modified to keep the spatial region captured by each coil to below half the field-of-view, then it may be possible to further improve reconstructions. Additionally, it may be possible to design the coil sensitivity such that the phase varies in a way that ensures the overlap between the multiple aliased copies occurs out-of-phase at all spatial locations.

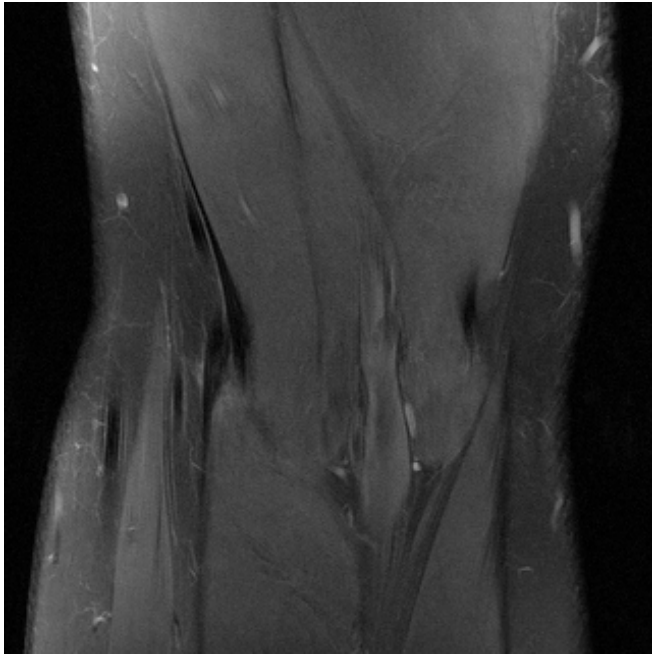
Acknowledgements

This work was made possible through close collaboration with the fastMRI team at Facebook AI research, including Nafissa Yakubova, Anuroop Sriram, Jure Zbontar, Larry Zitnick, Mark Tygert, Suvrat Bhooshan and Tullie Murrell,

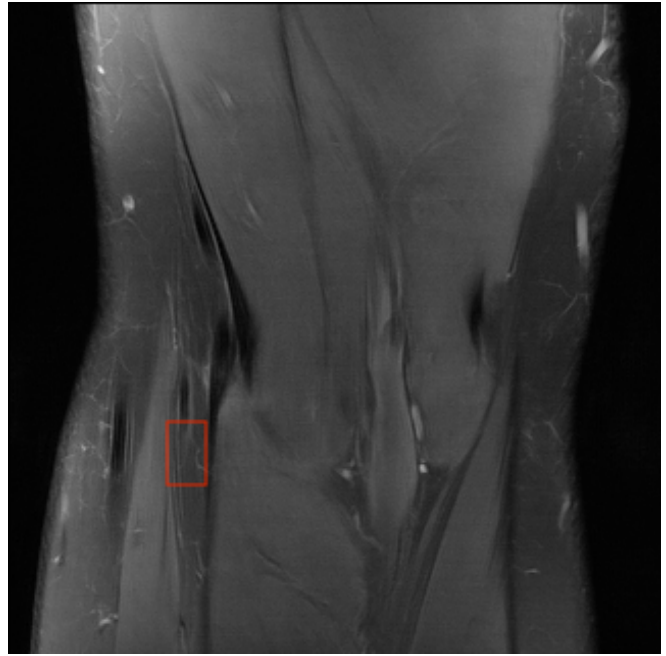
and our collaborators at NYU Langone Health on the fastMRI project [Zbontar et al., 2018], with special thanks to Florian Knoll, Matthew Muckley, Daniel Sodickson and Michael Recht.

References

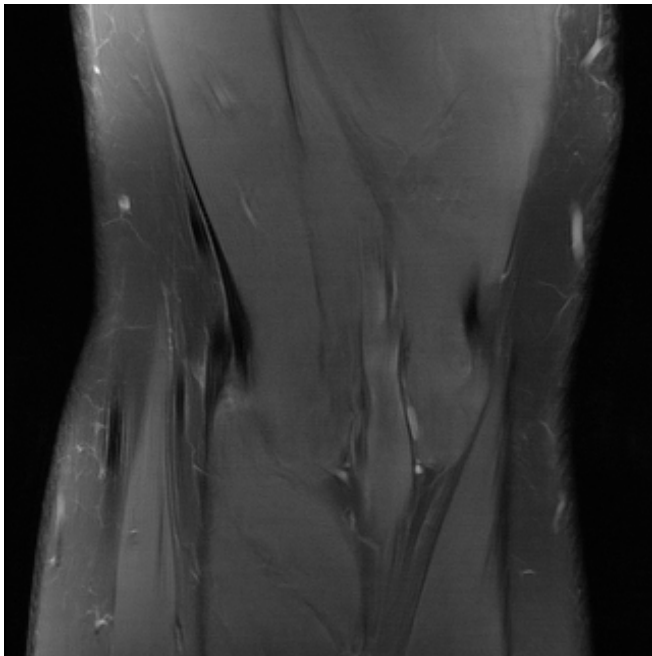
- Anagha Deshmane, Vikas Gulani, Mark A. Griswold, and Nicole Seiberlich. Parallel mr imaging. *Journal of Magnetic Resonance Imaging*, 36(1):55–72, 2012. doi: 10.1002/jmri.23639.
- David A. Feinberg, James D. Hale, Jeffrey C. Watts, Leon Kaufman, and Alexander Mark. Halving mr imaging time by conjugation: demonstration at 3.5 kg. *Radiology*, 1986.
- Mark A. Griswold, Peter M. Jakob, Robin M. Heidemann, Mathias Nittka, Vladimir Jellus, Jianmin Wang, Berthold Kiefer, and Axel Haase. Generalized autocalibrating partially parallel acquisitions (grappa). *Magnetic Resonance in Medicine*, 47(6), 2002.
- EM Haacke, ED Lindskog, and W Lin. A fast, iterative, partial-fourier technique capable of local phase recovery. *Journal of Magnetic Resonance (1969)*, 92(1):126–145, 1991.
- Michael Lustig, David Donoho, and John M. Pauly. Sparse mri: The application of compressed sensing for rapid mr imaging. *Magnetic Resonance in Medicine*, 2007.
- G. McGibney, M. R. Smith, S. T. Nichols, and A. Crawley. Quantitative evaluation of several partial fourier reconstruction algorithms used in mri. *Magnetic Resonance in Medicine*, 1993.
- Klaas P. Pruessmann, Markus Weiger, Markus B. Scheidegger, and Peter Boesiger. Sense: Sensitivity encoding for fast mri. *Magnetic Resonance in Medicine*, 42(5), 1999.
- Olaf Ronneberger, Philipp Fischer, and Thomas Brox. U-net: Convolutional networks for biomedical image segmentation. In Nassir Navab, Joachim Hornegger, William M. Wells, and Alejandro F. Frangi, editors, *Medical Image Computing and Computer-Assisted Intervention – MICCAI 2015*. Springer International Publishing, 2015.
- Jo Schlemper, Jose Caballero, Joseph V. Hajnal, Anthony N. Price, and Daniel Rueckert. A deep cascade of convolutional neural networks for mr image reconstruction. *IEEE TRANSACTIONS ON MEDICAL IMAGING*, VOL. 37, NO. 2, abs/1703.00555, 2018.
- Takayuki Yamamoto, Tomohisa Okada, Yasutaka Fushimi, Akira Yamamoto, Koji Fujimoto, Sachi Okuchi, Hikaru Fukutomi, Jun C. Takahashi, Takeshi Funaki, Susumu Miyamoto, Aurélien F. Stalder, Yutaka Natsuaki, Peter Speier, and Kaori Togashi. Magnetic resonance angiography with compressed sensing: An evaluation of moyamoya disease. *PLOS ONE*, 2018.
- Jure Zbontar, Florian Knoll, Anuroop Sriram, Matthew J. Muckley, Mary Bruno, Aaron Defazio, Marc Parente, Krzysztof J. Geras, Joe Katsnelson, Hersh Chandarana, Zizhao Zhang, Michal Drozdal, Adriana Romero, Michael Rabbat, Pascal Vincent, James Pinkerton, Duo Wang, Nafissa Yakubova, Erich Owens, C. Lawrence Zitnick, Michael P. Recht, Daniel K. Sodickson, and Yvonne W. Lui. fastMRI: An open dataset and benchmarks for accelerated MRI. 2018.



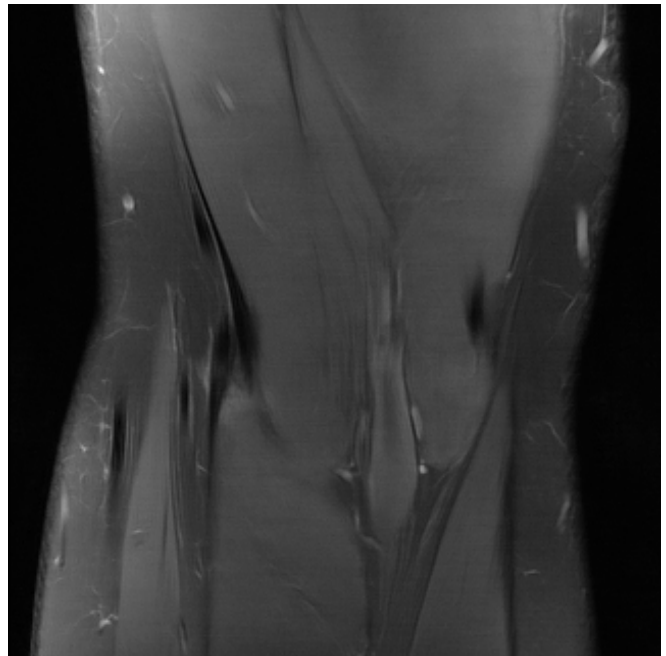
(a) Fully sampled ground truth



(b) Offset 0 sampling



(c) Offset 1 sampling



(d) Random sampling

Figure 3: Comparison of reconstructions from deep-learning based systems trained using identical model architectures, and differing sampling procedures, with areas of significant difference highlighted.



(a) Fully sampled ground truth



(b) Offset 0 sampling



(c) Offset 1 sampling



(d) Random sampling

Figure 4: In this example the offset-0 sampling mask loses detail in the smaller highlighted region. The detail differs significantly in the larger highlighted region, where the ground truth is also unclear. Images are best viewed at full resolution on a high-brightness monitor.



(a) Fully sampled ground truth



(b) Offset 0 sampling

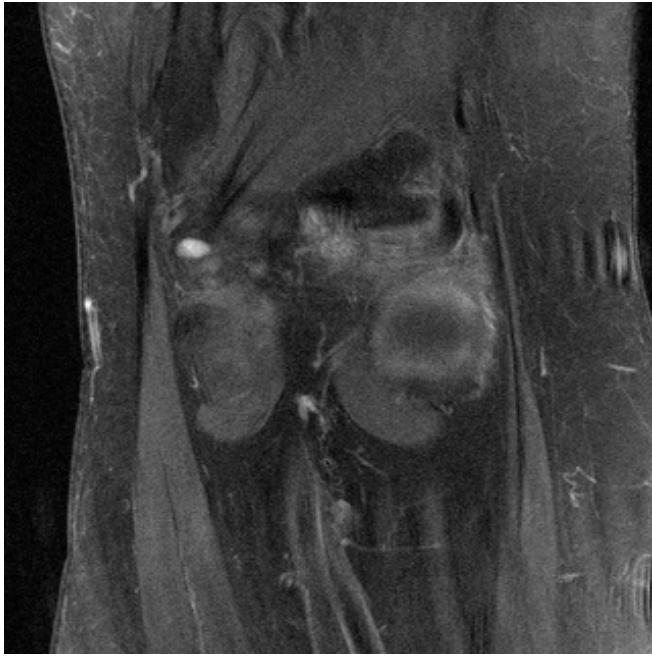


(c) Offset 1 sampling

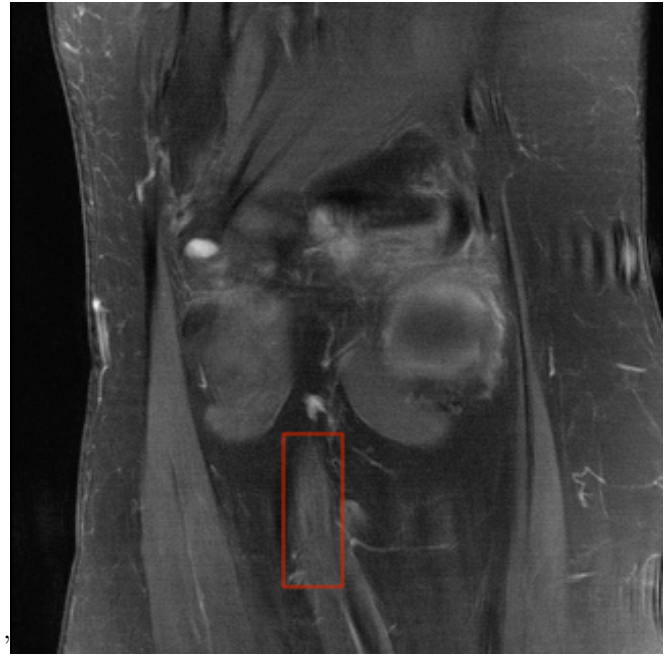


(d) Random sampling

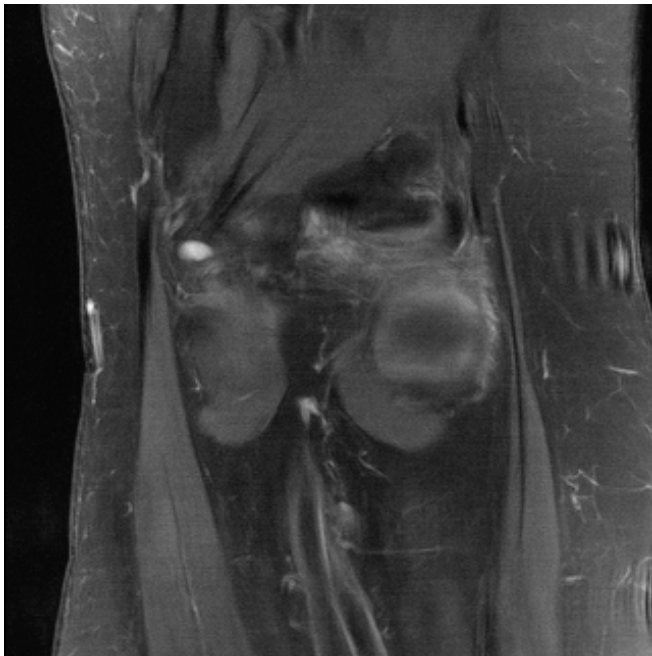
Figure 5: This example illustrates a low-noise situation where differences are less obvious. The fine detail throughout the bone is better captured by offset-1 sampling, compared to the highlighted region of the offset-0 version. There are clear differences in detail shown in the central high-lighted region.



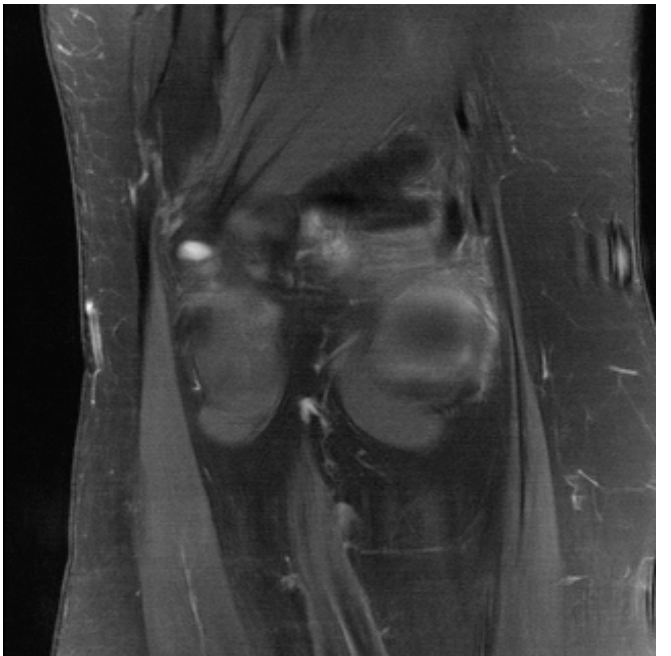
(a) Fully sampled ground truth



(b) Offset 0 sampling



(c) Offset 1 sampling



(d) Random sampling

Figure 6: This example illustrates the larger differences seen in high-noise situations. The offset-1 sampling mask retains large-scale structure compared to the offset-0 sampling mask in the highlighted region.